Exciton-scaling and optical excitations of self-similar phenylacetylene dendrimers

Evgeni Y. Poliakov, Vladimir Chernyak, Sergei Tretiak, and Shaul Mukamel
Department of Chemistry and Rochester Theory Center for Optical Science and Engineering, University of Rochester, P.O. RC Box 270216, Rochester, New York 14627-0216

(Received 13 November 1998; accepted 29 January 1999)

The collective electronic oscillators method is used to construct an effective Frenkel exciton Hamiltonian for conjugated dendrimers with fractal geometry. Self-similarity and the high degree of symmetry utilized by decomposing the space of optical excitations into irreducible representations make it possible to compute the one-exciton states and the linear optical response with reduced numerical effort that scales linearly rather than exponentially with the number of generations. The linear optical response is dominated by localized excitons belonging to the periphery. © *1999 American Institute of Physics.* [S0021-9606(99)51916-8]

I. INTRODUCTION

Advances in organic synthesis yield supermolecules with precisely defined structures. These include molecular rods and wires,[1–3] dendrimeric nanostructures,[4–8] higher fullerenes and metallofullerenes,[9,10] giant cagelike receptors,[11,12] and organic superlattices.[13] In addition, molecular aggregates are common in biological processes such as light-harvesting complexes in photosynthesis.[14] X-ray and NMR techniques provide the geometry of these structures which contain thousands of atoms.[15–18]

Optical spectroscopy is an important tool in the study of photophysics and photochemistry,[19] charge and energy transfer,[20] intermolecular interactions, and bonding in these systems. The theoretical investigation is complicated by the delocalized nature of electronic excitations, strong electron correlations, and vibronic coupling.[21,22] Application of quantum chemistry methods to calculate the electronic structures is limited by computational power to small systems.[21,22] The problem is simplified considerably for molecular aggregates made of well separated chromophores, whose interactions are purely Coulombic. Electron exchange is then negligible, each chromophore retains its own electrons, and the system may be described using the Frenkel exciton Hamiltonian.[23,24]

The electronic states and spectra of aggregates are simply related to those of their chromophore units. The situation is much more complex when the electronic states are delocalized across the entire molecule such as in the family of dendrimeric molecules shown in Fig. 1 (top panel). The linear absorption spectra of these dendrimers have recently been calculated using the collective electronic oscillator (CEO) approach, which only requires a moderate computational effort.[25,26] The resulting electronic normal modes are directly related to excited state charge distributions and motions of electrons and holes.[27,28] Real-space analysis then determines the underlying coherence sizes such as the sizes of electron-hole pairs created upon optical excitation, and helps identify the ''pieces'' of the whole molecule where these pairs (excitons) are confined.

Our previous calculations had shown that the linear absorption spectrum of each member of this dendrimeric family is dominated by a single peak at frequency close to that of a linear segment, in agreement with experiment.[29,30] This has been attributed to the localization of optical excitations on the linear segment, i.e., electron (and hole) exchange among segments is blocked.[28] Since charge transfer across meta-substitutions is negligible, the optical excitation can be modeled as a collection of weakly interacting two-level chromophores. The weak exciton transfer across meta-substitutions and the charge localization on the segments justifies the modeling of optical excitations as Frenkel excitons, which are tightly bounded electron-hole pairs (see bottom panel in Fig. 1).

In Sec. II, we construct the Frenkel exciton Hamiltonian and calculate its parameters by using the CEO technique. The properties of one-exciton states are discussed in Sec. III. In Appendix C we demonstrate how the one-exciton eigenvalue problem is simplified considerably by decomposing the Frenkel exciton Hamiltonian onto a set of Hamiltonians of much lower dimensionality. The symmetry properties of dendrimeric molecules described in Appendix B and in Sec. III A make this decomposition possible. The absorption spectra are calculated in Sec. IV, where we further analyze the nature of optical localization and the types of excitons contributing to the absorption spectra. The absorption line shape and other physical quantities are expressed in terms of wavefunctions of an effective linear chain using a mapping of the one-exciton wavefunctions described in Appendix A. The self-similar properties of dendrimers lead to unusual physical properties. As an example, in Sec. V, we show that the superradiant coherence size has a unique scaling dependence with molecular size. Finally, our results are summarized in Sec. VI.

II. FRENKEL EXCITON MODEL FOR DENDRIMERS

The first five members of the family of compact phenylacetylene dendrimers[29,31,32] are presented in the top panel of Fig. 1. The treelike molecules are formed by phenylacetylene segments[33] connected at the meta-position. We denote

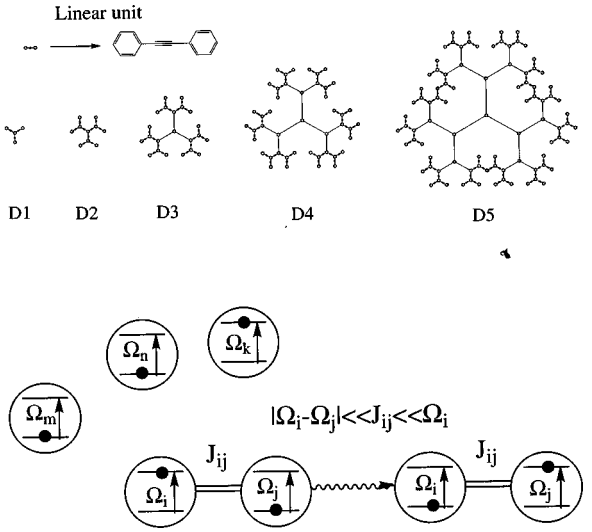

FIG. 1. Upper trace: Structures of the compact phenylacetylene dendrimers family made of the same linear building unit. Lower trace: Schematic representation of the Frenkel exciton model in molecular aggregates. The weakly coupled two-level chromophores have frequencies Ω_i, and J_{ij} denotes their coupling strength.

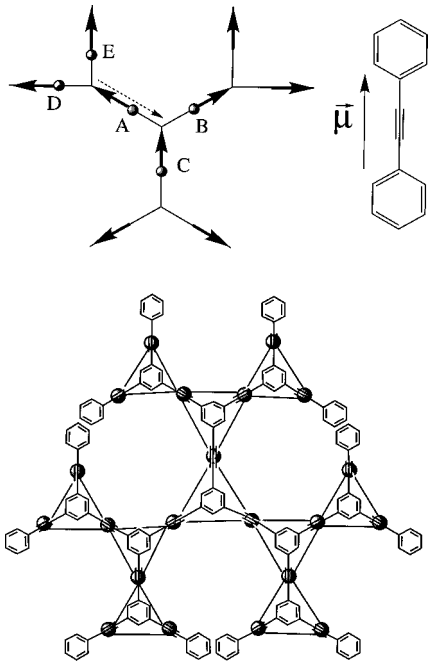

FIG. 2. Upper trace: The nearest-neighbor interaction model (NN) for the chromophores and the spatial orientation of the transition dipoles. The shaded dots denote the two-level chromophores, arrows represent the dipole orientation. Lower trace: Dual Bethe lattice with triangular cycles of nearest-neighbor interactions.

the dendrimer with l generations as Dl. Strictly speaking, the dendrimeric geometry is three-dimensional and packing considerations require it to become nonplanar, i.e., spheroidal, as the number of its generations increases.[34] However, since rotational symmetry along the acetylene unit is maintained, we shall model the optical properties assuming a two-dimensional planar geometry.

As shown in Ref. 28, optical excitations in these dendrimers are localized and involve no charge transfer between different segments. The Frenkel exciton model should therefore be applicable, i.e., each segment (bond) can be considered as a two-level chromophore (the ground and excited states of a single phenylacetylene chain). However, despite the localization of electron-hole pairs on single segments, the optically induced charge redistributions on different segments do interact. This Coulomb interaction gives rise to coherent energy transfer between chromophores, as illustrated in the bottom panel of Fig. 1. The relative motion of the electron and hole in each pair is localized on the various chromophores whereas their center of mass is delocalized. Such excitations are known as Frenkel excitons.[23,24,35]

The Frenkel exciton Hamiltonian for an assembly of two-level chromophores coupled by Coulomb interactions has a form,[23,24,35]

$$H=\sum_{\bar{n}} \Omega_{\bar{n}} B_{\bar{n}}^{\dagger} B_{\bar{n}} + \sum_{\bar{n}\neq\bar{m}} J_{\bar{n}\bar{m}} B_{\bar{m}}^{\dagger} B_{\bar{n}}, \tag{1}$$

where $B_{\bar{m}}$ ($B_{\bar{m}}^{\dagger}$) is the annihilation (creation) operator of an excitation localized on the $\bar{m}$-th chromophore. These operators satisfy the commutation relations

$$[B_{\bar{n}}, B_{\bar{m}}^{\dagger}] = \delta_{\bar{n}\bar{m}}(1-2B_{\bar{m}}^{\dagger} B_{\bar{m}}), \tag{2}$$

$$[B_{\bar{n}}, B_{\bar{m}}] = [B_{\bar{n}}^{\dagger}, B_{\bar{m}}^{\dagger}] = (B_{\bar{m}}^{\dagger})^2 = (B_{\bar{m}})^2 = 0. \tag{3}$$

We label the chromophores using Latin indices with an overbar. $\Omega_{\bar{n}}$ represents the transition energy from the ground state to the excited state of the $\bar{n}$-th chromophore. The Coulomb interaction between chromophores determines the hopping parameters $J_{\bar{n}\bar{m}}$.

The exciton model is depicted in Fig. 2, where the chromophores are denoted by shaded circles. All chromophores have the same transition frequencies $\Omega_{\bar{n}}=\Omega$ since the acetylene units are identical. The interaction $J_{\bar{n}\bar{m}}$ decreases rapidly with distance (scaling as $\sim 1/r_{\bar{m}\bar{n}}^3$, when the distance $r_{\bar{m}\bar{n}}$ between the $\bar{m}$-th and $\bar{n}$-th chromophores is much larger than the chromophore size); we can therefore neglect all Coloumb interactions between chromophores other than the nearest neighbors (NN) (i.e., chromophores whose linear units are connected through a phenyl ring). Connecting the nearest neighbors with lines leads to the dual Bethe lattice shown in the bottom panel of Fig. 2, which differs from the original Bethe lattice since it has triangle cycles. We thus describe optical excitations of a dendrimer by a Frenkel exciton aggregate with the dual Bethe lattice geometry.

By symmetry, the absolute magnitude of $J_{\bar{m}\bar{n}}$ between NN chromophores is the same. Determination of their signs is a more delicate matter. We first note that the excited state of any chromophore $\bar{m}$, and therefore the creation (annihilation) operators $B_{\bar{m}}^{\dagger}$ ($B_{\bar{m}}$) and the transition dipole $\mu_{\bar{m}}$, are defined up to a phase. The phase can be fixed up to a sign by requiring the transition dipoles to be real [see Eq. (23)]. The transition dipoles of the chromophores are directed along their corresponding linear units (Fig. 2). A sign change of the excited state wavefunction will reverse the direction of the transition dipole. Any choice of signs for the excited states generates a pattern of arrows of the same magnitude, which form 120 degrees angles. We have chosen to align the

$\bar{m}$-th dipole to point from the center of the dendrimer to its periphery as shown Fig. 2.

Since a sign change of a single arrow reverses the sign of the $B_{\bar{m}}$ and $B^{+}_{\bar{m}}$ operators of the corresponding chromophore, the sign of any NN interaction is determined by the relative orientation of the corresponding arrows. In particular, chromophore A in Fig. 2 interacts with four chromophores, B, C, D, and E. The signs of the AC, AD, and AE interactions are the same since they have the same relative configurations of the arrows with respect to the vertex representing the common phenyl ring: ''one in, one out.'' For the AB interaction, both arrows point out. This configuration can be transformed into ''one in, one out'' by changing the direction of the A-arrow. Since this procedure reverses the sign of the interactions we have $J_{AC}=J_{AD}=J_{AE}\equiv J$ and $J_{AB}\equiv -J$. In summary: The hopping parameter is given by J $(-J)$ for chromophores belonging to different (the same) generations.

In molecular aggregates the chromophores are well separated in space and their interactions J can, therefore, be calculated using electrostatic, e.g., dipole-dipole coupling. This is not the case for dendrimers where the chromophores overlap (they share a common phenyl ring) and are tightly bonded chemically. To compute J we examined the monomer (M), dimer (D), and trimer (T) dendrimeric units shown in Fig. 3 using the CEO procedure. The dimer and trimer have degenerate (or near degenerate) localized low-frequency electronic excitations whose weak interactions result in splitting of the spectrum. The remaining high-frequency electronic states are well separated and do not interfere with the lower transitions.

We start with the solution of the Frenkel exciton Hamiltonian for the dimer and trimer (see Fig. 3). This leads to the eigenvalue problem for 2×2 and 3×3 Hamiltonian matrices with all diagonal elements equal to Ω and all off-diagonal elements equal to J.

The dimer D has the symmetric and antisymmetric states

$$\Omega_{D1}=\Omega+J \quad \phi_{D1}=\frac{1}{\sqrt{2}}(\phi_1+\phi_2), \tag{4a}$$

$$\Omega_{D2}=\Omega-J \quad \phi_{D2}=\frac{1}{\sqrt{2}}(-\phi_1+\phi_2). \tag{4b}$$

The trimer T has three states; one is symmetric,

$$\Omega_{T1}=\Omega+2J \quad \phi_{T1}=\frac{1}{\sqrt{3}}(\phi_1+\phi_2+\phi_3), \tag{5a}$$

and the other two are degenerate,

$$\Omega_{T2}=\Omega-J \quad \phi_{T2}=\frac{1}{\sqrt{2}}(-\phi_1+\phi_2), \tag{5b}$$

$$\Omega_{T3}=\Omega-J \quad \phi_{T3}=\sqrt{\frac{2}{3}}(\phi_1/2+\phi_2/2-\phi_3). \tag{5c}$$

Here ϕ_1, ϕ_2, and ϕ_3 are the orthogonal excited state wavefunctions of the monomeric units.

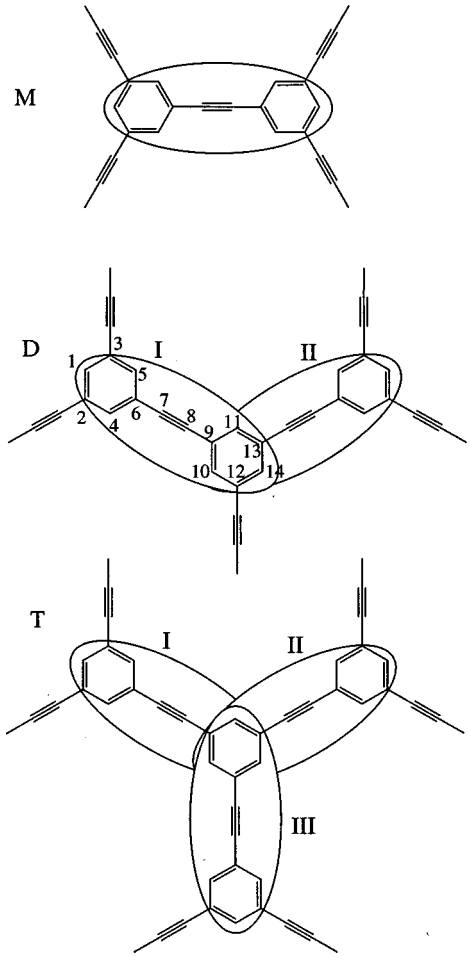

FIG. 3. Structures and atom labeling of phenyl acetylene monomer M, dimer D, and trimer T. Optimized AM1 level geometry yields the acetylene group parameters of $r_{6,7}=r_{8,9}=1.407$ Å, $r_{7,8}=1.200$ Å and phenyl group $r_{1,2}=r_{9,10}=1.403$ Å. Each monomeric unit is labeled starting from the outside phenyl. Note that the labels of the common phenyl are different for different linear units.

We have used the same average geometric parameters obtained at the AM1 level for all molecules (see Fig. 3). Note that even though the optical excitations are well localized within the linear segments, in the computations we retained the acetylene group at the *meta*-positions of the edge phenyls to model the chemical environments of *meta*-carbon atoms. The numerical procedure has been described in detail elsewhere.[25–28] The ZINDO code was first used to generate the INDO/S Hamiltonian.[36–39] We next calculated the Hartree-Fock ground-state density matrices[40,41] which are the input to the CEO/DSMA procedure[25,26] which computes the linear absorption spectra and the relevant *electronic normal modes* ξ_ν. Each mode is a matrix representing the electronic transition between the ground state $|0\rangle$ and an electronically excited state $|\phi_\nu\rangle$. Its matrix elements are given by

$$(\xi_\nu)_{mn}=\langle\phi_\nu|c^{+}_m c_n|0\rangle, \tag{6}$$

where $c^{+}_m(c_m)$ are creation (annihilation) operators of an electron at the m-th atomic orbital, and $|0\rangle$ $(|\phi_\nu\rangle)$ is the

TABLE I. Calculated low-frequency spectra of molecules displayed in Fig. 3. The dimer D and trimer T have two and three near-degenerate transition with central frequency Ω close to the monomer M band-edge transition. The splitting allows us to compute the coupling parameter J in the Frenkel exciton model [Eq. (1)].

	M	D	T
Ω_1 (eV)	3.603 723	3.594 700	3.586 112
Ω_2 (eV)		3.611 811	3.611 160
Ω_3 (eV)			3.611 160
Ω (eV)	3.603 723	3.603 255	3.602 811
$\Delta=\Omega_M-\Omega$ (cm^{-1})	0	3.77	7.35
J (cm^{-1})		−69.0	−67.3

ground (excited) state many-electron wavefunction. The eigenfrequencies Ω_ν of these equations provide the optical transition frequencies.[25,26]

The calculated low-frequency spectra summarized in Table I show an excellent agreement with predictions of the Frenkel model [Eqs. (4) and (5)]. The band-edge transition in the dimer spectrum splits into two peaks. This Davydov splitting ($2|J|$) gives $|J|=69\,cm^{-1}$. The central frequency shift ($3.77\,cm^{-1}$) is much smaller than J and reflects the weak coherence between linear units. The trimer calculations provide the sign of J (which is not available from the dimer) and further confirm our model. The sign is negative since the higher transition frequency corresponds to the doubly degenerate excited state. This molecule has three low-frequency transitions; two are completely degenerate as predicted by the Frenkel model. The calculated negative coupling $J=-67.3\,cm^{-1}$ agrees with that calculated for the dimer and is very close to the experimental estimate $J\sim 50\,cm^{-1}$ for M.[42] The central frequency shift ($7.37\,cm^{-1}$) is also much smaller than J. The one-exciton band-edge energy for the dimers and the trimers is $\Omega\approx 3.60$ eV. In all subsequent calculations, we have set $J=-68\,cm^{-1}$.

We next turn to the electronic modes ξ_ν [Eq. (6)]. If the Frenkel model holds, then each electronic mode of the aggregate should be a linear superposition of monomeric modes, for example,

$$(\xi_{T1})_{mn}=\langle\phi_{T1}|c_m^+c_n|0\rangle$$
$$=\frac{1}{\sqrt{3}}\langle(\phi_1+\phi_2+\phi_3)|c_m^+c_n|0\rangle$$
$$=\frac{1}{\sqrt{3}}(\xi_1+\xi_2+\xi_3). \qquad (7)$$

To test this relation we display the diagonal elements of the electronic modes in Fig. 4 using the carbon atom labeling of Fig. 3. The numbering for each linear unit starts at the external phenyl and ends on the common phenyl. Note that the same carbon atom on the common phenyl has different labels for different monomers. Panel D1 shows the diagonal elements of the electronic modes of $D1$ in the dimer and M in the monomer. The latter is multiplied by factor $1/\sqrt{2}$ [see Eq. (4a)]. The solid and dashed lines show units 1 and 2 of molecule D, respectively. The dotted line displays the molecule M. This plot shows that mode $D1$ corresponds to the symmetric state [see Eq. (4a)] and the coupling J is therefore negative. The monomer M mode virtually coincides with the dimer mode in units I and II outside the common phenyl. The difference on this phenyl is the result of superposition and interference. The mode of $D2$ is antisymmetric [compare with Eq. (4b)] and similar to the monomer M mode. The lowest frequency mode $T1$ is symmetric [compare with Eq. (5a)]. The next mode $T2$ is antisymmetric on the I and II units of the trimer and vanish on the unit III outside the common phenyl [see Eq. (5b)]. Mode $T3$ is symmetric and equal on I and II units, and antisymmetric with respect to unit III [compare with Eq. (5c)]. The electronic modes of the dimer and the trimer are thus given by linear superpositions of the monomeric modes, in agreement with Eqs. (4) and (5). These results confirm the applicability of the Frenkel exciton model.

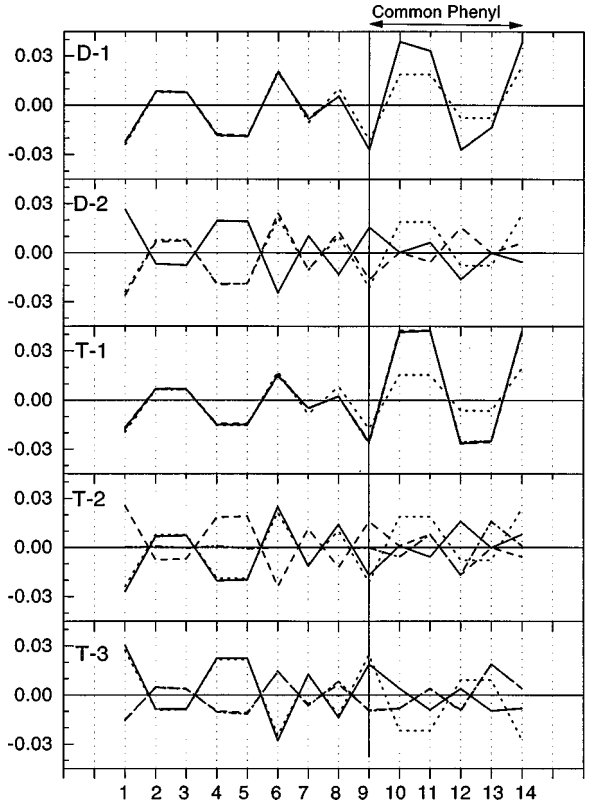

FIG. 4. Variation of the diagonal elements of low-frequency electronic modes listed in Table I. The x axis represents the carbon atoms (1–14) as labeled in Fig. 3. Each panel displays a single mode of dimer or trimer, shown solid [ξ(I)], dashed [ξ(II)], or dot-dashed line [ξ(III)] for each monomer unit. The dotted line represents the diagonal elements of the monomer M mode multiplied by correspondent factor [see Eqs. (4) and (5)]. Linear units I, II, and I–III of the dimer and trimer, respectively, are shown in Fig. 3.

III. PROPERTIES OF ONE-EXCITON STATES

A. Symmetry and classification of excitons

The one-exciton states can be found by diagonalizing the one-exciton subspace of the Hamiltonian [Eq. (1)]. The strong symmetry allows us to reduce the diagonalization of a huge $3\cdot(2^l-1)\times 3\cdot(2^l-1)$ matrix, where l is the number of generations, to the diagonalization of matrices no

larger than $l \times l$. Each generation is formed by a collection of phenylacetylene units separated by a fixed number of meta-conjugations. A walker which starts at the center should turn 60 degrees on the meta-conjugated linear units to reach to the next generation. The number of phenyls on the surface of a given generation (and linear chromophore segments) scales with generation number j as

$$N_j = 3 \cdot 2^{j-1}. \tag{8}$$

The total number of chromophores in Dl is $N = \Sigma_{j=1}^{l} N_j = 3(2^l - 1)$.

Interaction among chromophores results in delocalization of the optical excitations over the entire molecule, and the formation of excitons. We label the one-exciton eigenstates by Greek indices with an overbar, e.g., $\overline{\alpha}$. The one-exciton wavefunctions are

$$|\phi_{\overline{\alpha}}\rangle = \sum_{\overline{i}} \phi_{\overline{\alpha}}(\overline{i}) B_{\overline{i}}^{\dagger} |0\rangle. \tag{9}$$

We denote the set of chromophores of the Dl dendrimer by X_l. The space of one-exciton states denoted in Appendix B by W_l is, according to Eq. (9), a vector space with basis set X_l. The one-exciton space W_l naturally forms a representation of the dendrimeric symmetry group G_l described in Appendix B. A standard procedure for making use of symmetry to diagonalize the Hamiltonian H starts with decomposing W_l into a direct sum of irreducible representations of G_l and applying the Schur's lemma.[43] The decomposition of W_l is carried out in Appendix B [Eq. (B6)], and the application of Schur's lemma is explained in Appendix C. Combining the results of these appendices yields the following structure of one-exciton states. The excitons can be partitioned into antisymmetric and symmetric classes which belong to the representations V_j and $\tilde{V}_k$, respectively, in the decomposition of Eq. (B6). The antisymmetric excitons can be labeled by pairs of indices $\overline{m}\alpha$, where $\overline{m}$ is the chromophore where an exciton starts, while α is energy quantization number. For each $\overline{m} \in X_l$, $|\overline{m}|$ denotes the generation number to which $\overline{m}$ belongs (see Appendix B for an exact definition) and $\alpha = 1,2,\ldots,l-|\overline{m}|$. The wavefunction of an exciton which originates at $\overline{m}$ is shown in Fig. 5 where $j = l - |\overline{m}|$. All wavefunctions $\phi_{\overline{m}\alpha}(\overline{n})$ which originate in $\overline{m}$ are nonzero for $\overline{n} > \overline{m}$ only (see Appendix B for the formal definition of $\overline{n} > \overline{m}$), i.e., for $\overline{n}$ which belong to the branches which start at $\overline{m}$. As shown in the top panel in Fig. 5, a wavefunction $\phi_{\overline{m}\alpha}$ is determined by $j = l - |\overline{m}|$ numbers $\phi_{\alpha}^{(j)}(1), \ldots, \phi_{\alpha}^{(j)}(j)$.

The Schrödinger equation for $\phi_{\overline{\alpha}}$ given by Eq. (9),

$$H|\phi_{\overline{\alpha}}\rangle = \epsilon_{\overline{\alpha}}|\phi_{\overline{\alpha}}\rangle, \tag{10}$$

results in the system of equations [Eq. (A1)] for the coefficients $\phi_{\alpha}^{(j)}(1), \ldots, \phi_{\alpha}^{(j)}(j)$. In Appendix A we map the auxiliary eigenvalue problem (A1) onto the one-exciton states of an effective linear chain of length j with nearest-neighbor hopping [Eq. (A6)]. We, therefore, refer to the excitons $\phi_{\overline{m}\alpha}$ with $|\overline{m}| = l - j$ as excitons of the length j. Since an exciton of length j with a given quantum number α ($\alpha = 1,2,\ldots j$) can originate at any chromophore $\overline{m}$ with $|\overline{m}| = l - j$, we have $3 \cdot 2^{l-j-1}$ excitons with energy $\epsilon_{\alpha}^{(j)}$. This corresponds to the number of chromophores in the $l-j$ generation [see Eq. (8)]. The total number of excitons of length j is therefore $3 \cdot 2^{l-j-1} j$, where the last (j) factor is related to the quantum number α. According to the classification of Appendix B, excitons of length n form the space nV_n in the decomposition of Eq. (B6). The degeneracy of any system of length n according to Appendix C is given by $\dim V_n = 3 \cdot 2^{l-n-1}$, whereas the factor n gives the number of different energy values. Stated differently, there are n distinct excitons of length n whose wavefunctions are expressed in terms of n linear chain wavefunctions $\psi_{\alpha}^{(j)}$ (or $\phi_{\alpha}^{(j)}$) as illustrated in the top scheme in Fig. 5. Each of the distinct states has a $3 \cdot 2^{l-n-1}$-fold degeneracy.

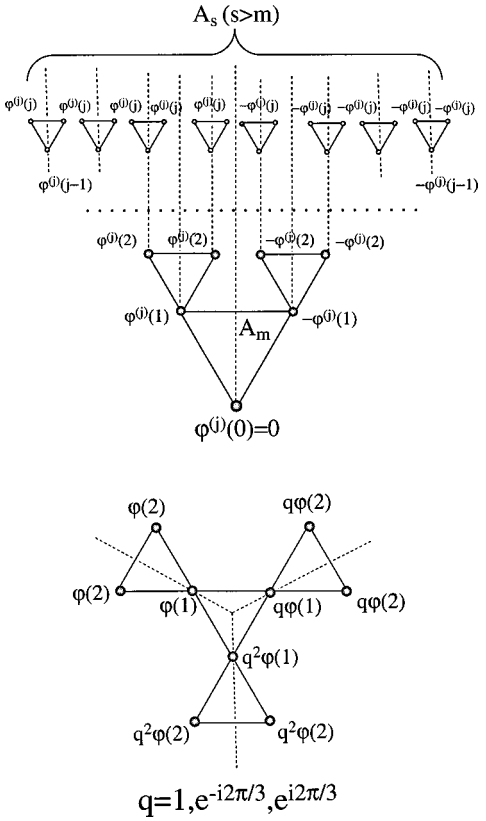

FIG. 5. Upper panel: The antisymmetric exciton of length j. The exciton wavefunction $\phi_{\alpha\overline{m}}$ is represented by $j = l - |\overline{m}|$ nonzero numbers $\phi^{(j)}(1),\ldots,\phi^{(j)}(j)$ (energy quantum number α's are dropped). Lower panel: Symmetric exciton and the representation of its wavefunction for the $D3$ molecule. (The subscripts for q_t and index α are dropped.)

The structure of the symmetric excitons is presented in the bottom scheme of Fig. 5. These excitons belong to the space $l\tilde{V}_1 \oplus l\tilde{V}_2 \oplus l\tilde{V}_3$ in the decomposition of Eq. (B6). They are labeled by the quantum numbers $q_t = e^{i2\pi(t-1)/3}$, with $t = 1,2,3$ in Eq. (A3) which correspond to the excitons belonging to $l\tilde{V}_1$, $l\tilde{V}_2$, and $l\tilde{V}_3$ with energies $\epsilon_{\alpha,t}, t = 1,2,3$, respectively, and $\alpha = 1,2,\ldots,l$. The auxiliary wavefunctions $\tilde{\phi}_{\alpha}^{(t)}$ which determine the exciton wavefunctions in the dendrimer satisfy Eqs. (A2). Equations (A2) are obtained by substituting the exciton wavefunction represented in terms of the auxiliary functions $\tilde{\phi}_{\alpha}^{(t)}$ in Fig. 5 into the Schrödinger equation. The eigenvalue problem [Eq. (A2)] is mapped in Appendix A onto an effective linear chain [Eq. (A6)]. Symmetric excitons are nondegenerate except of a trivial double

degeneracy with respect to the quantum number $t=2,3$ (i.e., $\epsilon_{\alpha,2}=\epsilon_{\alpha,3}$).

In summary, we have classified all one-exciton states of Dl by their symmetry and expressed their wavefunctions in terms of auxiliary wavefunctions of excitons in effective linear chains with nearest-neighbor hopping. We next discuss the density of states and the distribution of exciton sizes.

B. Density of one-exciton states

The density of states (DOS) provides the simplest characteristic of excitons. We consider three types of DOS. The local density of states at the $\overline{m}$-th chromophore is given by

$$\rho_{\overline{m}}(\omega)=\frac{1}{\pi}\mathrm{Im}[G_{\overline{mm}}(\omega)]. \tag{11}$$

Here ω is the energy (we set $\omega=0$ for the ground state), and the one-exciton Green's function is given by

$$G_{\overline{mn}}(\omega)=\sum_{\overline{\alpha}}\frac{\phi_{\overline{\alpha}}(\overline{m})\phi^{*}_{\overline{\alpha}}(\overline{n})}{\omega-\epsilon_{\overline{\alpha}}+i\Gamma}. \tag{12}$$

$\overline{\alpha}$ runs over all one-exciton states, and Γ is a dephasing rate.

The density of states for the i-th generation, $\rho_i(\omega)$, $i=1,\ldots,l$ is given by the sum over the density of states of all the chromophores belonging to that generation,

$$\rho_i(\omega)=\sum_{\overline{i}}^{|\overline{i}|=i}\rho_{\overline{i}}(\omega)=N_i\sum_{\overline{\alpha}}\frac{\Gamma|\phi_{\overline{\alpha}}(\overline{i})|^2}{(\omega-\epsilon_{\overline{\alpha}})^2+\Gamma^2}, \tag{13}$$

where N_i (number of chromophores in the i-th generation) is given by Eq. (8).

Finally, the total density of states $\rho(\omega)$ for the entire aggregate is given by

$$\rho(\omega)=\frac{1}{N}\sum_{\overline{m}=1}^{N}\rho_{\overline{m}}(\omega)=\frac{1}{N}\sum_{i=1}^{l}\rho_i(\omega), \tag{14}$$

with the normalization

$$\int_{-\infty}^{\infty}\rho(\omega)d\omega=1. \tag{15}$$

Using the exciton classification introduced in Sec. III A, we can separate Eq. (13) into the contributions of antisymmetric and symmetric exciton states

$$\rho_i(\omega)=\Gamma N_i\left(\sum_{s=1}^{l-1}\sum_{\alpha=1}^{j}\frac{|\phi^{(j)}_{\alpha}(i)|^2}{(\omega-\epsilon^{(j)}_{\alpha})^2+\Gamma^2}+\sum_{t=1}^{3}\sum_{\alpha=1}^{l}\frac{|\tilde{\phi}^{(t)}_{\alpha}(i)|^2}{(\omega-\epsilon_{\alpha,t})^2+\Gamma^2}\right). \tag{16}$$

Only the antisymmetric excitons that start earlier than the $(i-1)$-th generation (of length $s=1,\ldots,i-1$) contribute to the first summation in Eq. (16). The exciton of length s corresponds to the effective linear chain length $l-s$. Using the transformations (A12) and (A13) and the equivalence of the symmetric exciton states for $t=2$ and $t=3$, we obtain

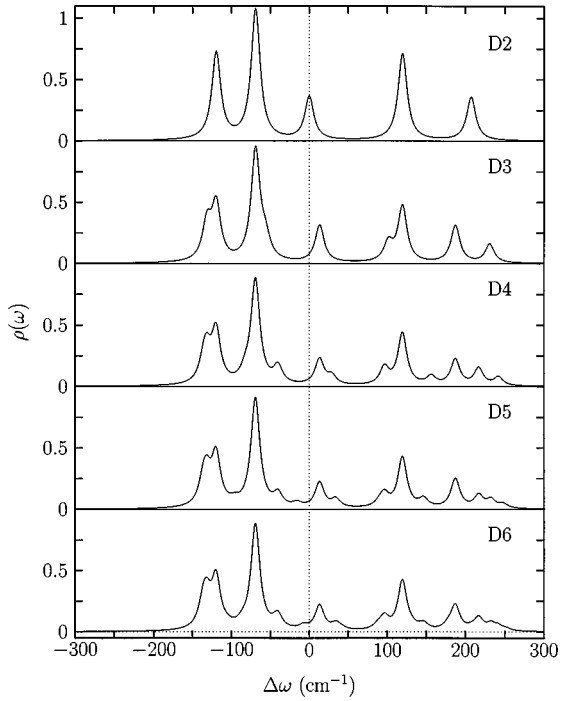

FIG. 6. The density of states as a function of frequency detuning from the resonance $\Delta\omega\equiv\omega-\Omega$ for dendrimers with different number of generations: $D2-D6$. The dephasing rate of all one-exciton states is $\Gamma=0.1|J|\sim 8\ \mathrm{cm}^{-1}$.

$$\rho_i(\omega)=\Gamma N_i\left(\sum_{s=1}^{i-1}\sum_{\alpha=1}^{l-s}2^{s-i}\frac{|\psi^{(l-s)}_{\alpha}(i-s)|^2}{(\omega-\epsilon^{(l-s)}_{\alpha})^2+\Gamma^2}+\frac{1}{3}\sum_{t=1}^{2}\sum_{\alpha=1}^{l}2^{1-i}\frac{t|\tilde{\psi}^{(t)}_{\alpha}(i)|^2}{(\omega-\epsilon_{\alpha,t})^2+\Gamma^2}\right). \tag{17}$$

Combining Eqs. (8) and (14) in (17), the density of states for the individual generations is given by

$$\rho_i(\omega)=\frac{\Gamma}{2^l-1}\left(\sum_{s=1}^{i-1}2^{s-1}\sum_{\alpha=1}^{l-s}\frac{|\psi^{(l-s)}_{\alpha}(i-s)|^2}{(\omega-\epsilon^{(l-s)}_{\alpha})^2+\Gamma^2}+\frac{1}{3}\sum_{t=1}^{2}\sum_{\alpha=1}^{l}\frac{t|\tilde{\psi}^{(t)}_{\alpha}(i)|^2}{(\omega-\epsilon_{\alpha,t})^2+\Gamma^2}\right). \tag{18}$$

The density of states for the entire molecule [Eq. (14)] as a function of the frequency detuning, $\Delta\omega\equiv\omega-\Omega$, is displayed using Fig. 6. We have calculated $\rho_i(\omega)$ using Eq. (18) with $\Gamma\sim 8\ \mathrm{cm}^{-1}$ and then found the density of states $\rho(\omega)$ by applying Eq. (14). To that end, we first diagonalized l matrices of type (A6): $l-1$ matrices with $\Omega_0=\Omega+J$ and $J=-|J|$ of size $i\times i$ $(i=1,\ldots,l-1)$ and the $l\times l$ matrix with $\Omega_0=\Omega-2J$ and $J=-|J|$ to find the energies and wavefunctions of linear chains. The one-exciton wavefunctions were then computed using Eqs. (A12) and (A13).

The DOS of $D2-D6$ are displayed in Fig. 6. It follows from the self-similarity of dendrimers that the spectrum of higher generation molecules contains all the features of lower generations. The DOS of a given generation contains therefore all the peaks of earlier generations, and the number of peaks increases with l. However, the DOS saturates at $l=5$, and $D5$ and $D6$ are very similar.

C. The participation ratio

The participation ratio provides a convenient measure of exciton size.[44–46] The participation ratio $P_{\bar{\alpha}}$ of an exciton $\bar{\alpha}$ is expressed in terms of its wavefunction $\phi_{\bar{\alpha}}$,

$$P_{\bar{\alpha}}=\frac{\Sigma_{\bar{m}}|\phi_{\bar{\alpha}}(\bar{m})|^4}{\Sigma_{\bar{m}}|\phi_{\bar{\alpha}}(\bar{m})|^2}. \tag{19}$$

If a wavefunction is uniformly distributed on k chromophores, Eq. (19) yields $P^{-1}=k$, which implies that the inverse participation ratio P^{-1} constitutes a measure for the number of chromophores on which an exciton is delocalized. The maximal value $P^{-1}=N$ is achieved for a wavefunction delocalized over the entire aggregate. In a dendrimer it can be reached by symmetric excitons only. For an antisymmetric exciton of length s the wavefunction can occupy no more than $2(2^s-1)$ chromophores (see Fig. 5), which gives the upper bound for P^{-1} of antisymmetric excitons of length s. The minimal value of $P^{-1}=1$ corresponds to an exciton which is fully localized on a single chromophore. Expressing the exciton wavefunctions in terms of the auxiliary linear chain wavefunctions by using Eqs. (A12) and (A13) and substituting them into Eq. (19), yields

$$P_\alpha=\sum_{i=1}^{s}\frac{|\psi_\alpha^{(s)}(i)|^4}{2^i},\quad \alpha=1,\ldots,s, \tag{20}$$

for antisymmetric excitons and

$$P_\alpha=\frac{2}{3}\sum_{i=1}^{l}\frac{|\tilde{\psi}_\alpha^{(t)}(i)|^4}{2^i},\quad t=1,2,\quad \alpha=1,\ldots,l, \tag{21}$$

for symmetric excitons. The participation ratio [Eq. (21)] is the same for the α-th state of $t=2$ and $t=3$ symmetric excitons, but differs for $t=1$ type due to the differences in the wavefunctions [Eq. (A2)].

In Fig. 7, we display the inverse participation ratios for $D2-D6$, calculated from Eqs. (20) and (21), versus their frequency detuning $\Delta\omega$. They vary between the localized ($P^{-1}=2$) and the delocalized ($P^{-1}=N$) values. The figure shows that one-exciton states with higher P^{-1} tend to occupy the band edges of the frequency interval. The frequency range of P^{-1} increases with l, reflecting the appearance of one-exciton states close to the band edges.

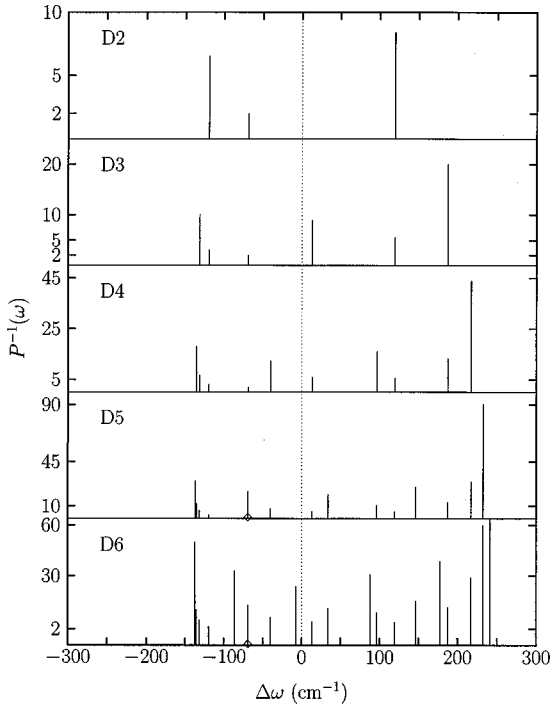

FIG. 7. The inverse participation ratios P^{-1} for $D2-D6$. The diamonds in the two bottom panels represent two-fold degeneracy of the state $\Delta\omega\approx-70\ \mathrm{cm}^{-1}$ in $D5$ and $D6$: one state with $P^{-1}=2$ is ''blocked'' by the other state with $P^{-1}\approx31$ in $D5$ and by $P^{-1}\approx20$ in $D6$. The highest peak for $D6$ is off-scale ($P^{-1}=180$).

IV. LINEAR ABSORPTION

Since the dendrimer size is typically much smaller than the optical wavelength, its interaction with incident field $\mathbf{E}$ is described in the dipole approximation,

$$H_{\mathrm{int}}=-\mathbf{P}\cdot\mathbf{E}, \tag{22}$$

with the polarization operator

$$\mathbf{P}=\sum_{\bar{m}}\mu_{\bar{m}}(B_{\bar{m}}^{\dagger}+B_{\bar{m}}), \tag{23}$$

and $\mu_{\bar{m}}=\langle\bar{m}|\mu|0\rangle$ denotes the transition dipole matrix element of the $\bar{m}$-th chromophore.

The linear susceptibility of an aggregate $\hat{\chi}^{(1)}(\omega)$ can be expressed in terms of one-exciton states,[35]

$$\hat{\chi}^{(1)}(\omega)=\sum_{\bar{\alpha}}\frac{\mu_{\bar{\alpha}}\mu_{\bar{\alpha}}^{*}}{\omega-\epsilon_{\bar{\alpha}}+i\Gamma}, \tag{24}$$

where the transition dipole moment of the α-th exciton is

$$\mu_\alpha=\sum_{\bar{m}}\mu_{\bar{m}}\phi_\alpha(\bar{m}), \tag{25}$$

and the direct product of the two vector dipoles in the right-hand side (r.h.s.) of Eq. (24) forms the tensor structure of $\hat{\chi}^{(1)}$. Restricting our calculations to unpolarized light (or to an ensemble of randomly oriented molecules), the absorption coefficient $\sigma(\omega)=\mathrm{Im\,Tr}[\hat{\chi}^{(1)}(\omega)]$ is given by

$$\sigma(\omega)=\sum_{\bar{\alpha}}\frac{\Gamma|\mu_{\bar{\alpha}}|^2}{(\omega-\epsilon_{\bar{\alpha}})^2+\Gamma^2}. \tag{26}$$

We partition the absorption into the sums of contributions from antisymmetric and symmetric excitons denoted $\sigma_s(\omega)$ and $\sigma_a(\omega)$, respectively,

$$\sigma(\omega)=\sigma_a(\omega)+\sigma_s(\omega). \tag{27}$$

Details of the calculations of $\sigma_a(\omega)$ and $\sigma_s(\omega)$ are given in Appendix D. Using Eqs. (D4) and (D9), we finally have

$$\sigma(\omega)=\sum_{s=1}^{l-1}\sum_{\alpha=1}^{s}\frac{|\mathbf{M}_\alpha^{(s)}|^2\Gamma}{(\omega-\epsilon_\alpha^{(s)})^2+\Gamma^2}+\frac{4}{3}\sum_{\alpha=1}^{l}\frac{|\mathbf{M}_\alpha^{(l)}|^2\Gamma}{(\omega-\epsilon_\alpha^{(l)})^2+\Gamma^2}. \tag{28}$$

In Fig. 8 we display absorption lineshapes of $D1$ to $D6$ (divided by the total number of chromophores). Calculations were made using the one-exciton wavefunctions and ener-

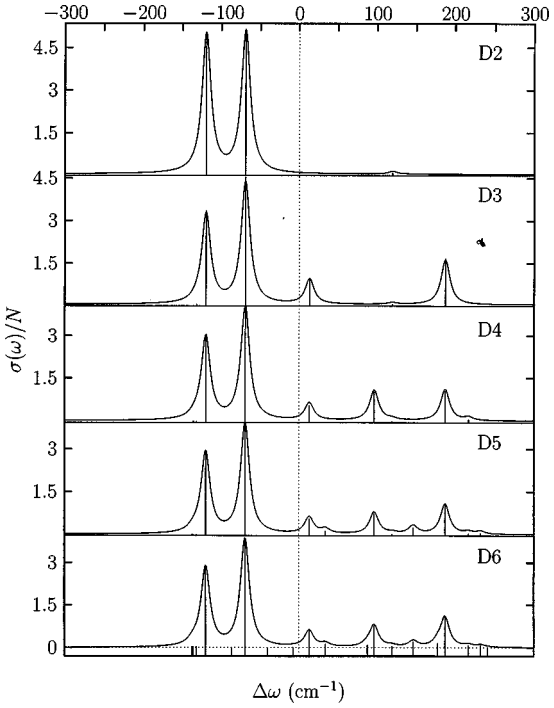

FIG. 8. Linear absorption (per chromophore) calculated from Eq. (28) for molecules with different number of generations. Peaks represent distinct one-exciton states.

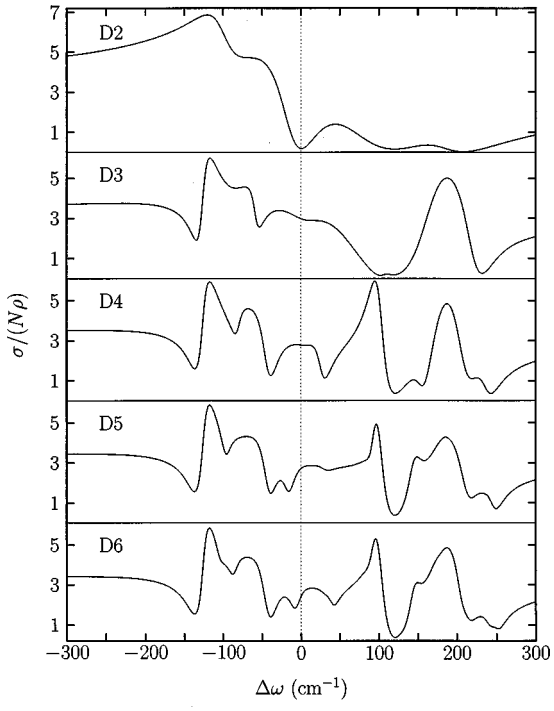

FIG. 9. The average oscillator strength per state $\sigma/(N\rho)$ is displayed versus frequency detuning for dendrimers of different generations ($D2-D6$).

gies given in Sec. III B and the dephasing rate $\Gamma=8\ \mathrm{cm}^{-1}$. The spectra converge at $D5$, and the spectra of $D5$ or $D6$ as well as higher Dl (not shown) look virtually identical. The high resolution ($\Gamma=0$) stick spectra shown as well have some small differences in their weak peaks.

The Dl spectrum has $l(l+1)/2$ peaks representing the various distinct one-exciton states. As a direct consequence of self-similarity, the absorption spectrum of a given generation shows all the features of lower-generation molecules plus l additional peaks.

We also note that the spectra are nonsymmetric around $\Delta\omega=0$. The highest peaks are located in the red ($\Delta\omega<0$). This is a consequence of the negative value of J, as in J aggregates.[47] The magnitude of the normalized absorption does not vary with generation, except for $D2$, where the absorption maxima are slightly stronger. This makes sense since the total number of excitons which contribute to the absorption increases as fast as the total number of chromophores (both double for successive generations).

The oscillator strength per one-exciton state, given by the ratio of normalized absorption and the one-exciton density, $\sigma/(N\rho)$, is displayed in Fig. 9 for $D2-D6$. Its variation over the entire frequency range is weak and does not exceed ~ 7.

Similar to Fig. 8, Dl contains the peaks of $D(l-1)$ plus additional peaks. We further note that $\sigma/(N\rho)$ approaches 3 from below for large positive detunings ($\Delta\omega<0$). The same limiting value is reached from above for large negative detunings. We have calculated $\sigma/(N\rho)$ averaged over $\Delta\omega$ for $D2-D6$. The average ratios turn out to be close to 3 as well: $\sigma/(N\rho)\approx 2.84\pm 0.60$ for $D5$ and $\sigma/(N\rho)\approx 2.91\pm 0.40$ for $D6$.

The number of peaks of $\sigma/(N\rho)$ increases with l. This is because there are more one-exciton states in molecules with higher l. As a result, the local maxima occur at $\Delta\omega \approx 100\ \mathrm{cm}^{-1}$ in $D4$ in comparison with the absolute minima in $D2$ and $D3$. However, once a certain local maximum occurs at $D(n-1)$, it is repeated for dendrimers Dl with $l \geqslant n$. This again follows from self-similarity.

Figure 10 displays the normalized absorption, σ/N, one-exciton density of states, $\rho(\omega)$, the oscillator strength per one-exciton state, $\sigma/(N\rho)$, and the inverse participation ratio $P^{-1}(\omega)$ for $D5$. Using the figure, we can identify the excitons that dominate the absorption and show where they reside. The bottom panel shows that the exciton resonances span a $5.4|J|$ bandwidth ($\Delta\omega$ varies between $-2|J|$ and $3.4|J|$). For an infinite dendrimer ($l\to\infty$), as a comparison, the exciton band spans the region $[-(1+2\sqrt{2})J,(2\sqrt{2}-1)J]$, which gives a $\sim 5.8|J|$ bandwidth.

The upper bound for the inverse participation ratio is obtained for a state uniformly delocalized over the entire molecule and is equal to the total number of chromophores N. For $D5$, this is the state at $\omega\approx\Omega+3.4|J|$ with $P^{-1}=93$. This state has a very weak contribution to the absorption (peak j). The strongest peaks a and b correspond to the other extremes with $P^{-1}=3$ and 2, respectively. $P^{-1}=2$ corresponds to a localized state where the exciton is equally distributed on the two chromophores. These antisymmetric excitons of unit length occupy the periphery of the molecule. Peaks c and h are produced by excitons of length $j=3$ with $P^{-1}=6$ and 13, respectively. Our analysis shows that localized excitons which belong to the molecular periphery are responsible for the strong absorption peaks. The delocalized

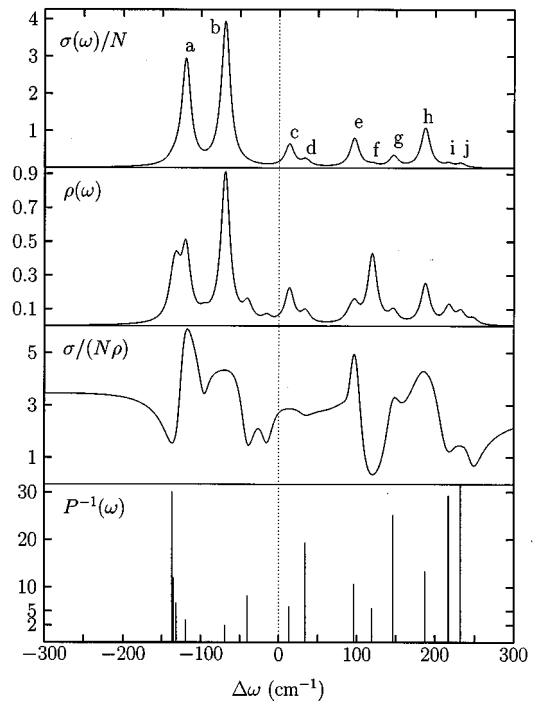

FIG. 10. Characteristics of the absorption spectrum of $D5$. The panels (from top to bottom) are the absorption coefficient normalized to the total number of chromophores, σ/N, density of the one-exciton states, $\rho(\omega)$, the average dipole strength, $\sigma/(N\rho)$, and inverse participation ratio, $P^{-1}(\omega)$. The frequencies and their participation ratios $(\Delta\omega, P^{-1})$ of the absorption peaks are (a) $(-120,3)$, (b) $(-70,2)$, (c) (13, 6), (d) (34, 19), (e) (97, 11), (f) (120, 6), (g) (145, 25), (h) (187, 13), (i) (217, 29), (j) (235, 93). P^{-1} of the 235 cm^{-1} peak is off-scale ($P^{-1}=93$).

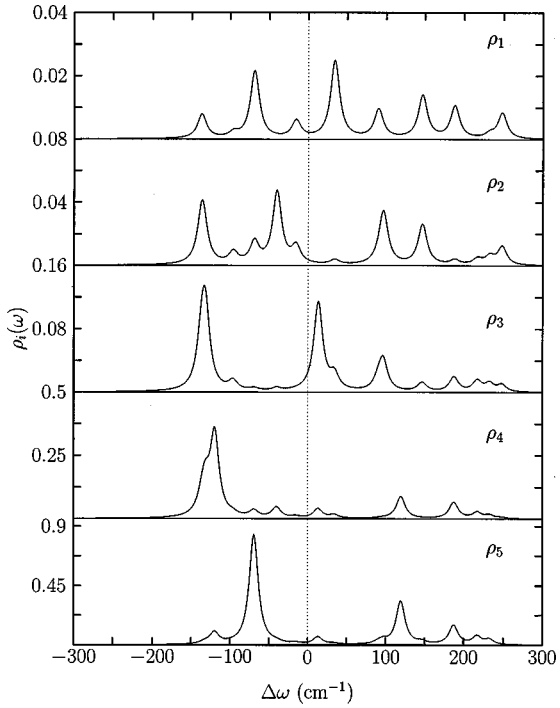

FIG. 11. Density of states, $\rho_i(\omega)$, of the various generations of $D5$.

states in contrast lead to a much weaker absorption. A similar behavior has been previously found in biological light-harvesting complexes.[48,49]

It is instructive to note that for all four excitons which dominate the absorption spectrum the values of the inverse participation ratio P^{-1} are close to the maximal values allowed by the exciton symmetry determined by its length. The $j=1$ exciton (peak b) reaches its maximal possible value $P^{-1}=2$, the $j=2$ exciton (peak a) has $P^{-1}=3$ with the maximal possible value $P^{-1}=6$, finally the two $j=3$ excitons (peaks c and h) have $P^{-1}=6,13$ versus the maximal value $P^{-1}=14$ for $j=3$ excitons. This implies that the four excitons dominating the absorption spectrum are localized over the entire regions allowed by their symmetry. Stated differently, the dominant excitons are localized because of the dendrimer symmetry rather than dynamical effects.

Comparison of the top two panels in Fig. 10 shows that the high density of one-exciton states usually correlates with strong absorption. The one-exciton densities for individual generations ρ_i in $D5$ are displayed in Fig. 11. The figure shows that the states which belong to the chromophores of the last, periphery, generation give the leading contribution to $\rho(\omega)$ (bottom panel). Since there are more excitons of shorter lengths in every ρ_i, these excitons should dominate the absorption spectrum, provided their oscillator strengths are not too weak.

Figure 10 also demonstrates that the correlation between the absorption and density of states does not always hold. For example, the high density ρ does not result in strong absorption in the f region (top panel) since the oscillator strength is very low. As seen, $\sigma/(N\rho)\leqslant 0.5$ at frequency $\omega \approx \Omega+\sqrt{3}|J|$ $(\Delta\omega\approx 120\,\text{cm}^{-1})$, so that even the relatively large number of states (12) for exciton of length $j=2$ does not lead to a peak in the absorption coefficient (compare the second and third panels from the top in Fig. 10). In contrast, the oscillator strengths of the shortest excitons are sufficiently high, and combined with the high density of states, these excitons give the leading contribution to the absorption σ in Figs. 8 and 10.

Figures 11 and 12 display the individual generation density of states $\rho_i(\omega)$. These quantities play a key role in the real space picture of energy transfer in the excited state (i.e., the redistribution of excitons among generations). Generally the density of states should be dominated by the contribution of the highest generation $\rho_l(\omega)$ because of the exponential growth of the number of chromophores in a generation N_j toward the periphery. Figure 11 demonstrates, however, that in certain frequency regions the density of one-exciton states for the chromophores that belong to $i=4$ and even $i=3$ can locally dominate the one-exciton density, as shown in the second and the third panels from the bottom in Fig. 11. They lead to local maxima of the normalized absorption produced by excitons of length $j=2$ at frequency $\Omega-\sqrt{3}|J|$ and $j=3$ at $\sim\Omega+0.2|J|$. The dominance of the density of states for the highest generation ρ_l over all the other generations, except for two regions where ρ_{l-1} and ρ_{l-2} are larger locally, is common to dendrimeric molecules of any length. This is illustrated in Fig. 12, which shows the same

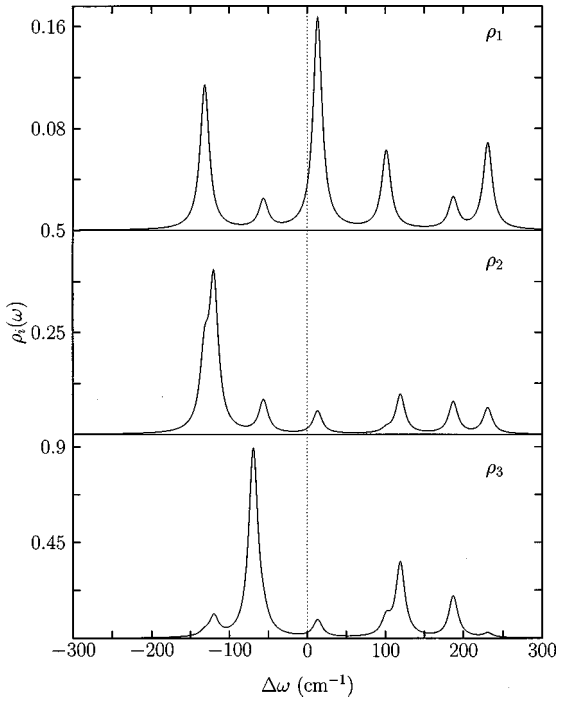

FIG. 12. Densities of one-exciton states, ρ_i, for the various generations of $D3$.

features for $D3$. The main peaks of ρ_1 and ρ_2 are at $\Delta\omega \approx 13$ and $\Delta\omega \approx -125\,\mathrm{cm}^{-1}$, respectively.

V. SCALING AND SUPERRADIANT FRACTAL DIMENSION

The superradiant factor L_s of an aggregate is defined as the ratio of its radiative decay rate to that of a monomer. It is proportional to the squared dipole moment of the transition between the lowest, scale-invariant, excited state and the ground state.[50] In this section we compare the superradiance factor of a dendrimer with that of an ordinary, translationally invariant aggregate. If Ψ_1 is the wavefunction of the lowest one-exciton state of a dendrimer, we can use Eq. (9) to express the superradiance factor as

$$L_s = \langle \Psi_1 | \mu | 0 \rangle^2 = \left| \sum_{\bar{m}} \mu_{\bar{m}} \phi_1(\bar{m}) \right|^2, \tag{29}$$

where we set the dipole moment magnitudes $|\mu_{\bar{m}}| = 1$ for all $\bar{m}$. The maximal superradiant factor is obtained when all the dipoles are parallel, so that

$$L_s = \left| \sum_{\bar{m}} |\phi_1(\bar{m})| \right|^2. \tag{30}$$

It is shown in Appendix A that the one-exciton wavefunctions can be mapped onto the wavefunctions of a linear chain. In the limit of very long chains ($l \to \infty$), we obtain an energy band, with a discrete state at $\epsilon = 2J$. For a negative hopping parameter $J < 0$, the energy of the discrete state is the lowest, and the one-exciton wavefunctions scale exponentially with the generation number as $\phi_1(i) \propto 2^{-i}$, $i \in 1, \ldots, l$. The total number of wavefunctions is proportional to 2^i [see, for example, the normalization of (A4) and (A5)]. These two factors cancel and contributions from different generations are the same, so that $\Sigma_{\bar{m}} |\phi_1(\bar{m})| \propto l$, and Eq. (30) gives

$$L_s \propto l^{D_s}, \quad D_s = 2. \tag{31}$$

For comparison, let us consider a translationally invariant lattice in D dimensions. The lowest wavefunction amplitude is proportional to $1/\sqrt{N}$, where N is the total number of sites. Therefore, Eq. (30) gives $L_s \propto N$. The total number of sites depends on the characteristic size l of the system as $N \propto l^D$. We thus obtain $D_s = D$.

Dendrimers can be viewed as a collection of one-dimensional linear chains. In that sense they are quasi-one-dimensional. However, the number of chromophores grows exponentially with generation as in infinite-dimensional systems. Its fractal dimension defined as the logarithmic ratio of particle number and some scaling length,[51] can be defined $d \equiv \log N / \log l \sim l / \log l \to \infty$ with l [see Eq. (8)]. This ''mixed'' dimensionality results in the unusual superradiant factor: The scaling exponent D_s neither equals unity as expected for one-dimensional structures nor is infinite. There is a profound reason why $D_s = 2$. Dendrimers are scale-invariant rather than translationally invariant objects. Consequently, generations with an exponentially increasing number of chromophores still contribute equally to the superradiant factor (31).

VI. SUMMARY

We have studied the linear optical properties of phenylacetylene dendrimers, which are macromolecules with self-similar geometry. The molecule can be viewed as a weakly interacting ensemble of nearest neighbor, two-level chromophores. The Frenkel-exciton model usually applied for molecular aggregates may be used to describe their one-excitons states and optical excitation. The collective electronic oscillator approach has been utilized to establish this model for dendrimers and to calculate its parameters. Strong symmetry originating from self-similarity was used to find the one-excitons states (both energies and wavefunctions) with considerably reduced computational effort. In a Dl molecule with l generations, the number of chromophores increases exponentially as $N = 3(2^l - 1)$. However, by employing the irreducible representations, we were able to avoid the tedious diagonalization of Hamiltonian with dimension $N \times N$. The problem has been reduced to diagonalization of $l-1$ matrices of $i \times i$ dimension ($i = 1, \ldots, l-1$) and 2 matrices of $l \times l$ dimension. The merits of the irreducible representation approach should be especially noticeable in calculations of nonlinear susceptibilities.

We find that the strongly localized one-exciton states dominate the linear absorption, as in light-harvesting complexes. Such states occupy the molecular periphery and represent excitons of the shortest lengths. Periphery states make the dominant contribution to the absorption since the number of such states is the largest. Based on the irreducible repre-

sentation analysis, we characterize the main absorption peaks in terms of exciton lengths and participation ratios.

A dendrimer can be viewed as a collection of linear chains. This allows us to express its optical properties in terms of linear-chain wavefunctions. However, the optical properties of dendrimers are very different from those of linear systems. Scale invariance of self-similar objects such as dendrimers can lead to a nontrivial scaling dependence of physically measured quantities with molecular size. The $L_s \sim l^2$ scaling of the superradiant factor L_s with size is different from the expected $L_s \sim l$ dependence for one-dimensional structures. Although the number of atoms grows exponentially with generation, each generation still contributes equally to the superradiant factor by virtue of the scaling of the oscillator strength.

ACKNOWLEDGMENTS

We wish to thank Professor F. Cohen for useful discussions of symmetry properties of dendrimeric molecules. Helpful comments of Professor R. Kopelman and Professor Y. Klafter are most appreciated. This research was supported by the Air Force Office of Scientific Research (Grant No. F49620-96-1-0030), and the National Science Foundation (Grants No. CHE-9526125 and No. PHY94-15583).

APPENDIX A: CALCULATION OF ONE-EXCITON WAVEFUNCTIONS

The absorption coefficient and other parameters such as one-exciton density and the participation ratio needed for the linear absorption analysis given in Secs. III and IV require the knowledge of one-exciton states. In this Appendix we solve the eigenvalue problem for the two classes of excitons introduced in Sec. III A by mapping it onto an effective eigenvalue problem for a set of linear chains.

1. Systems of one-exciton wavefunctions in dendrimers

Using the structure of antisymmetric one-exciton wavefunctions described in Sec. III A (see Fig. 5), the Schrödinger equation [Eq. (10)] adopts the form of a system of linear equations for the antisymmetric excitons of length j,

$$
\begin{aligned}
&(\Omega-\epsilon_\alpha^{(j)}+J)\,\phi_\alpha^{(j)}(1)+2J\phi_\alpha^{(j)}(2)=0,\\
&(\Omega-\epsilon_\alpha^{(j)}-J)\,\phi_\alpha^{(j)}(m)+J[\,\phi_\alpha^{(j)}(m+1)\\
&\qquad+2\,\phi_\alpha^{(j)}(m-1)]=0,\quad m=2,\ldots,j-1,\\
&(\Omega-\epsilon_\alpha^{(j)}-J)\,\phi_\alpha^{(j)}(j)+J\phi_\alpha^{(j)}(j-1)=0.
\end{aligned}
\tag{A1}
$$

For symmetric excitons, we obtain in a similar way

$$
\begin{aligned}
&(\Omega-\epsilon_{\alpha,t}-J[q_t+q_t^2])\,\tilde{\phi}_\alpha^{(t)}(1)+2J\tilde{\phi}_\alpha^{(t)}(2)=0,\\
&(\Omega-\epsilon_{\alpha,t}-J)\,\tilde{\phi}_\alpha^{(t)}(m)+J[\,\tilde{\phi}_\alpha^{(t)}(m+1)\\
&\qquad+2\,\tilde{\phi}_\alpha^{(t)}(m-1)]=0,\quad m=2,\ldots,j-1,\\
&(\Omega-\epsilon_{\alpha,t}-J)\,\tilde{\phi}_\alpha^{(t)}(j)+J\tilde{\phi}_\alpha^{(t)}(j-1)=0,\\
&\qquad q_t=e^{i2\pi(t-1)/3},\quad t=1,2,3,
\end{aligned}
\tag{A2}
$$

where $\epsilon_{\alpha,t}$ is the symmetric exciton energy. Note that system (A2) describes all three branches of symmetric excitons, and the energy manifold is the same for different branches.[52]

The linear systems (A1) and (A2) only differ by the first equation. When $t=2$ and $t=3$, $q_t+q_t^2\equiv -1$, the two systems become identical. By solving (A1) in general and (A2) for the case $t=1$ $(q_t=1)$, one can find the energies and the wavefunctions of the symmetric and antisymmetric excitons. The antisymmetric exciton wavefunctions are normalized as

$$
\sum_{i=1}^{j} 2^i\,|\phi_\alpha^{(j)}(i)|^2=1,\quad \forall\,\alpha,
\tag{A4}
$$

whereas the wavefunctions of symmetric exciton of length l are normalized as

$$
\sum_{i=1}^{j} 3\cdot 2^{j-1}\,|\tilde{\phi}_\alpha^{(t)}(i)|^2=1,\quad \forall\,\alpha,t=1,2,3.
\tag{A5}
$$

2. Mapping the eigenvalue problem onto a linear chain

The dendrimer geometry is not linear. However, due to the zigzag structure of its segments, the one-exciton states can be modeled using a collection of linear chains with variable lengths. The linear systems (A1) and (A2) for the one-exciton symmetric and antisymmetric wavefunctions can be conveniently mapped onto the eigenvalue problem of a linear chain.

We consider a linear chain of length j. We further enumerate the wavefunctions for each bond from left to the right as $\psi_\alpha(1),\psi_\alpha(2),\ldots,\psi_\alpha(j)$, where α represents different energies. The system of equations for the linear chain wavefunctions can be obtained directly from (A2) and (A1),

$$
\begin{aligned}
&(\Omega_0-\omega_\alpha)\,\psi_\alpha(1)+J\sqrt{2}\,\psi_\alpha(2)=0,\\
&(\Omega'-\omega_\alpha)\,\psi_\alpha(m)+J\sqrt{2}[\,\psi_\alpha(m+1)\\
&\qquad+\psi_\alpha(m-1)]=0,\quad m=2,\ldots,j-1,\\
&(\Omega'-\omega_\alpha)\,\psi_\alpha(j)+J\sqrt{2}\,\psi_\alpha(j-1)=0,
\end{aligned}
\tag{A6}
$$

We look for a solution of Eqs. (A6) in the form of a standing wave

$$
\psi_\alpha(m)=A_\alpha e^{ik_\alpha m}+B_\alpha e^{-ik_\alpha m}.
\tag{A7}
$$

Substitution of (A7) into the second equation of system (A6) results in the dispersion relationship between the energy ω_α and the wavevector k_α,

$$
\omega_\alpha=2\sqrt{2}J\cos k_\alpha+\Omega.
\tag{A8}
$$

By substituting (A7) into the first and the third equations of (A6), we obtain the quantization of the wavevector k,

$$\frac{\sin(k[j+1])}{\sin(kj)}=\frac{\Omega_0-\Omega}{J\sqrt{2}}, \tag{A9}$$

and the relationship between the coefficients A_α and B_α,

$$B_\alpha=-A_\alpha e^{2ik_\alpha}\frac{\Omega_0-\omega_\alpha+J\sqrt{2}e^{ik_\alpha}}{\Omega_0-\omega_\alpha+J\sqrt{2}e^{-ik_\alpha}}. \tag{A10}$$

From the normalization condition $\Sigma_{i=1}^{j}|\psi_\alpha(i)|^2=1$ and Eq. (A10), we obtain

$$|A_\alpha|^2=\frac{2J^2-(\Omega'-\omega_\alpha)(\Omega_0+\omega_\alpha)}{4\sqrt{2}J\,\Sigma_{i=1}^{l}\{\sqrt{2}J\sin[k_\alpha(i-2)]+(\Omega_0-\omega_\alpha)\sin[k_\alpha(i-1)]\}^2}. \tag{A11}$$

These linear-chain wavefunctions can be used to construct the one-exciton wavefunctions of dendrimers. The wavefunctions of antisymmetric excitons of length j [system (A1)] are related to the wavefunctions of the linear chain [Eq. (A6)] by

$$\phi_\alpha^{(j)}(i)=\psi_\alpha^{(j)}(i)/\sqrt{2^i}, \tag{A12}$$

with substitutions $\Omega_0=\Omega+J$, $\Omega'=\Omega-J$ $\epsilon_\alpha^{(j)}=\omega_\alpha$. The symmetric excitons of length l are similarly given by

$$\tilde{\phi}_\alpha^{(t)}(i)=\tilde{\psi}_\alpha^{(t)}(i)/\sqrt{3\cdot 2^{i-1}}, \tag{A13}$$

and the substitution $\Omega_0=\Omega-J(q_t+q_t^2)$, $\Omega'=\Omega-J$, $\epsilon_{\alpha,t}=\omega_\alpha$. The mapping of the original eigenvalue problem is established by noting that the substitution of Eqs. (A12) and (A13) into Eqs. (A1) and (A2), respectively, yields Eq. (A6).

APPENDIX B: SYMMETRY GROUP AND IRREDUCIBLE REPRESENTATIONS OF A FINITE DENDRIMER

Here we describe the symmetry group properties of a dendrimeric molecule and use them to decompose the original one-exciton space W_l onto irreducible representation subspaces. Although the number of chromophores and sites in a dendrimer grows exponentially with its size (number of generations) l [see Eq. (8)], its strong symmetry allows us to compute optical signals by inverting matrices of a maximal size $l\times l$. In this section we introduce the symmetry group G_l for a Dl dendrimer and describe its relevant representations which are used in calculations of the linear optical responses.

We start by introducing the necessary definitions. Let X_l be the set of chromophores (sites) of Dl. For $\bar{m}\in X_l$, we define its absolute value $|\bar{m}|\in Z$ as the generation number to which $\bar{m}$ belongs (the generations are labeled from the center to the boundary). X_l has a structure of a partially ordered set: we say that $\bar{m}\geqslant\bar{n}$ if $|\bar{m}|\geqslant|\bar{n}|$, and $\bar{m}$ belong to the branch which starts at $\bar{n}$. The symmetry group of G_l of a dendrimer is a subgroup of transformations for the chromophore set X_l, i.e., a subgroup of all the permutations for X_l. The group G_l is generated by the set of transformations $A_{\bar{n}}$, $\bar{n}\in X_l$ and B, defined as follows: $A_{\bar{n}}$ flips the two branches which start at $\bar{n}$, while all the other elements of X_l remain unchanged. Transformation B rotates the dendrimer with respect to the center by $2\pi/3$. The generators $A_{\bar{n}}$ and B satisfy the following relations:

$$B^3=I,\quad A_{\bar{m}}^2=I,\quad \forall\bar{m}\in X_l, \tag{B1}$$

$$A_{\bar{m}}A_{\bar{n}}=A_{A_{\bar{m}}(\bar{n})}A_{\bar{m}}\quad \text{for } \bar{m}\leqslant\bar{n},$$

$$A_{\bar{m}}A_{\bar{n}}=A_{\bar{n}}A_{A_{\bar{n}}(\bar{m})}\quad \text{for } \bar{n}\leqslant\bar{m},$$

$$A_{\bar{m}}A_{\bar{n}}=A_{\bar{n}}A_{\bar{m}}\quad \text{otherwise}, \tag{B2}$$

$$BA_{\bar{m}}=A_{B(\bar{m})}B,\quad \forall\bar{m}\in X_l, \tag{B3}$$

where I is the unit operator. Equation (B1) shows that either three subsequent rotations or two flips of the same branch do not change the structure of the molecule. Commutation relationships (B2) show how two flips of branches which are either inserted into each other or are independent can be interchanged. The equivalence between rotation with further flip and a subsequent flip around the rotated branch (operation $A_{B(\bar{m})}$) with subsequent rotation of the whole molecule is given by Eq. (B3). The group G_l is uniquely defined by its generating elements $A_{\bar{m}}$, B, and the relations (B1)–(B3).

It is easy to see that the effective Frenkel-exciton Hamiltonian introduced in Sec. II does not change under the transformations of the group G_l. This implies that G_l is the symmetry group for our problem.

Irreducible representations of G_l can be classified by sequential applications of the construction for irreducible representations of semidirect products of groups.[53] However, we do not need all irreducible representations, and therefore the complete classification goes beyond the scope of this paper.

The basic object in our calculations is the one-exciton space W_l whose states are the functions on X_l. A natural action of G_l on W_l induced by the action of G_l in X_l is given by $g\phi(\bar{m})=\phi(g^{-1}\bar{m})$, $g\in G_l$, $\phi\in W_l$. The one-exciton Hamiltonian (1) is obviously both linear operator in W_l and symmetric with respect to G_l. Diagonalization of the one-exciton Hamiltonian h to get the one-exciton states is based on the Schur's lemma, which is outlined in Appendix C. To apply the Schur's lemma for the above purpose, W_l should

be decomposed into a direct sum of irreducible representations of G_l. The remainder of this Appendix is devoted to this problem.

We first construct the irreducible representations $V_1, V_2, \ldots, V_{l-1}$; $\tilde{V}_1, \tilde{V}_2, \tilde{V}_3$, which participate in the decomposition of W_l. $\tilde{V}_t$ $(t=1,2,3)$ is a one-dimensional representation generated by the vector $\hat{v}_t$ with the following action of G_l:

$$A_{\bar{m}}\tilde{v}_t=\tilde{v}_t, \quad B\tilde{v}_t=e^{i2\pi(t-1)/3}\tilde{v}_t. \tag{B4}$$

In particular, $\tilde{V}_1$ is the unit representation of G_l. The representation V_n, $n=1,2,\ldots,l-1$, has the dimensions $\dim V_n = 3\cdot 2^{l-n-1}$ and is generated by the vectors $v_n^{(\bar{m})}$ with $\bar{m} \in X_l$ and $|\bar{m}|=l-n$ with the following action of the group generators:

$$\begin{aligned} &Bv_n^{(\bar{m})}=v_n^{(B(\bar{m}))}, \quad A_{\bar{m}}v_n^{(\bar{m})}=-v_n^{(\bar{m})}, \\ &A_{\bar{n}}v_n^{(\bar{m})}=v_{\bar{n}}^{(\bar{m})} \quad \text{for } \bar{n}>\bar{m}, \\ &A_{\bar{n}}v_n^{\bar{m}}=v_n^{(A_{\bar{n}}(\bar{m}))} \quad \text{otherwise.} \end{aligned} \tag{B5}$$

A direct check shows that the action of the generators (B4) and (B5) is consistent with the relations (B1)–(B3) which completes the construction. It is also easy to show that the representations V_n and $\tilde{V}_k$ are irreducible. These irreducible representations participate in the decomposition of W_l in the following way. The vector $v_n^{(\bar{m})}$ is represented by the functions ϕ with $\phi(\bar{k})\neq 0$ for $\bar{k}>\bar{m}$ only, which satisfy the conditions $A_{\bar{m}}\phi=-\phi$, $A_{\bar{s}}\phi=\phi$ for $\bar{s}>\bar{m}$; their space is n-dimensional according to the number of generations from $|\bar{m}|+1$ to l. This implies that V_n occurs n times in the decomposition. Each representation $\tilde{V}_k$ occurs l times in the decomposition; vectors $\tilde{v}_t$ are represented by the wavefunctions with $A_{\bar{n}}\phi=\phi$ and $B\phi=\exp(i2\pi(t-1)/3)\phi$. We then have

$$W_l=\oplus_{n=1}^{l-1} nV_n \oplus l\tilde{V}_1 \oplus l\tilde{V}_2 \oplus l\tilde{V}_3, \tag{B6}$$

where

$$nV=\underbrace{V\oplus V\oplus\cdots\oplus V}_{n}.$$

The formal proof of Eq. (B6) can be completed by a direct check that the functions ϕ representing the vectors $v_n^{(\bar{m})}$ and $\tilde{v}_j$ in W_l are orthogonal to each other and by comparing the dimensions of both sides of Eq. (B6).

Finally we note that the Dl symmetry group G_l can be expressed using the construction of iterated wreath product. Introducing H_l as the symmetry group of one of the three branches of the Dl group of one of the three branches of the Dl dendrimer, we can express G_l as a semidirect product

$$G_l=Z_3 \wr (H_l\times H_l\times H_l), \tag{B7}$$

with respect to the action of Z_3 on $H_l\times H_l\times H_l$ given by cyclic permutations. H_l can be defined inductively: $H_2=Z_2$ and

$$H_l=Z_2 \wr (H_{l-1}\times H_{l-1}), \tag{B8}$$

where Z_2 acts on $H_{l-1}\times H_{l-1}$ as the group of permutations of two elements. H_l can be also considered as a 2-Sylow subgroup of the group of the permutations of 2^l elements.

APPENDIX C: MATRIX PROJECTION ONTO IRREDUCIBLE REPRESENTATION SUBSPACE

In this section we outline the Schur's lemma and apply it to diagonalize the Frenkel exciton Hamiltonian described in Sec. II. Instead of diagonalizing a matrix of $3(2^l-1)\times 3(2^l-1)$ dimension, only up to $l\times l$ matrices are required for Dl.

As discussed in Appendix B, the one-exciton space W_l can be decomposed onto the direct sum of its subspaces (irreducible representations $V_1, V_2, \ldots, V_i$). Irreducible representation V_i $(i<l)$ is invariant with respect to the original space W, does not intersect with another, and does *not* contain any subspaces V_{i_j} which are invariant with respect to V_i. Suppose that the irreducible representation of dimension m, V_m, occurs n times, so that $W=\oplus nV_m$. According to the Schur's lemma,[43] matrix h_{mn} of dimensionality $mn\times mn$ in the subspace V_m can be represented by a matrix formed by m blocks; each block is occupied by the $n\times n$ matrix Λ_{ij}

$$h_{mn}=\begin{pmatrix} \Lambda_{11}\Lambda_{12}\ldots\Lambda_{1m} \\ \cdots \\ \Lambda_{n1}\Lambda_{n2}\ldots\Lambda_{nm} \end{pmatrix}. \tag{C1}$$

The matrices Λ_{ij} are diagonal

$$\Lambda_{ij}=\begin{pmatrix} \lambda_{ij},0,0\ldots 0 \\ 0,\lambda_{ij},0\ldots 0 \\ \cdots \\ 0,0,0\ldots\lambda_{ij} \end{pmatrix}. \tag{C2}$$

It is easy to see from Eqs. (C1) and (C2) that the original matrix h_{mn} of dimension $mn\times mn$ is equivalent to the matrix h_{ij} of dimension $n\times n$,

$$h_{ij}=\begin{pmatrix} \lambda_{11},\lambda_{12},\ldots\lambda_{1n} \\ \cdots \\ \lambda_{n1},\lambda_{n2},\ldots\lambda_{nn} \end{pmatrix}. \tag{C3}$$

The Frenkel exciton Hamiltonian (1) has dimensionality $\bar{\alpha}\times\bar{\alpha}$, where $\bar{\alpha}$ represents all one-exciton states. However, in the subspace of each representation V_k, the matrix dimension is lowered considerably to $k\times k$. Due to decomposition (B6), the eigenvalue problem for the Hamiltonian (1) is equivalent to the eigenvalue problem for $l-1$ matrices h of dimension $i\times i$ for each representation V_i $(i=1,\ldots,l-1)$ and three matrices of dimension $l\times l$ (representations $\tilde{V}_1$, $\tilde{V}_2$, and $\tilde{V}_3$). Thus, using group symmetry properties the diagonalization of system (11) eventually reduces to diagonalization of $l-1$ matrices (A1) and 2 matrices (A2) of dimension $l\times l$ (see the details in Appendix A).

APPENDIX D: ONE-EXCITON CONTRIBUTIONS TO THE ABSORPTION COEFFICIENT

In Eq. (27), we have separated the absorption coefficient $\sigma(\omega)$ onto symmetric $\sigma_s(\omega)$ and antisymmetric $\sigma_a(\omega)$ con-

tributions. In this Appendix we express these contributions in terms of one-exciton states.

Using the notation of Sec. III A for Eq. (25), the transition dipole for antisymmetric excitons is

$$|\mu_\alpha^{(s)}| = \left| \sum_{\bar{m}} \mu_{\bar{m}} \phi_\alpha^{(s)}(\bar{m}) \right|. \tag{D1}$$

Equation (26) only depends on the absolute value of the transition dipole for each exciton state (D1) and is independent on its relative orientation. There are $n_s = 3 \cdot 2^{l-1-s}$ antisymmetric excitons of length $s \in [1, l-1]$. The absolute magnitudes of the transition dipole moments $|\mu_\alpha^{(s)}|$ are identical for all n_s states of the same s and α in Eq. (26). This gives

$$\sigma_a(\omega) = 3 \cdot 2^{l-1} \Gamma \sum_{s=1}^{l-1} 2^{-s} \sum_{\alpha=1}^{s} \frac{|\mu_\alpha^{(s)}|^2}{(\omega - \epsilon_\alpha^{(s)})^2 + \Gamma^2}. \tag{D2}$$

The dipoles $\mu_{\bar{m}}$ are directed from the center toward the vertexes in each equilateral triangle of a given exciton, and their mutual directions form 120 degree angles in space as shown in Fig. 2 (top panel). The absolute values of $\mu_{\bar{m}}$ are the same, but the wavefunctions are antisymmetric with respect to inversion around exciton origin $A_{\bar{m}}$ (or the axis that divides the exciton space by half) in the top panel of Fig. 5. As a result, the vector projection of $\mu_\alpha^{(s)}$ onto the $A_{\bar{m}}$ axis vanishes. It can be shown by induction that the transition dipole for exciton of length s equals $\mu_\alpha^{(s)} = \pm 2 \cos(\pi/6) \Sigma_{j=1}^{s} \phi_\alpha^{(s)}(j) \mathbf{e}_x^{(s)}$, where $\mathbf{e}_x^{(s)}$ is the unit vector that is perpendicular to $A_{\bar{m}}$ and belongs to the exciton plane. Using Eq. (A12), the dipole moment for the α-th state is given in terms of the linear chain wavefunctions

$$\mu_\alpha^{(s)} = \mp \sqrt{3} \sum_{j=1}^{s} \frac{\psi_\alpha^{(s)}(j)}{\sqrt{2^j}} \mathbf{e}_x^{(s)}, \tag{D3}$$

where $\mp$ corresponds to the case when $\mathbf{e}_x^{(s)}$ is directed from the left to right in the exciton plane, or vice versa.

Substitution of Eq. (D3) into (D2) gives the contribution of antisymmetric excitons to the absorption coefficient

$$\sigma_a(\omega) = \Gamma \sum_{s=1}^{l-1} \sum_{\beta=1}^{s} \frac{|\mathbf{M}_\alpha^{(s)}|^2}{(\omega - \epsilon_\alpha^{(s)})^2 + \Gamma^2}, \tag{D4}$$

where the transition dipole moment magnitude of the α-th antisymmetric state in the exciton of length s is defined as

$$|\mathbf{M}_\alpha^{(s)}|^2 = 9 \cdot 2^{l-s-1} \left| \sum_{j=1}^{s} 2^{-j/2} \psi_\alpha^{(s)}(j) \right|^2, \quad \alpha = 1, \ldots, s. \tag{D5}$$

It follows from Eq. (26) and the exciton properties described in Sec. III A that the symmetric part of absorption can be written as

$$\sigma_s(\omega) = \Gamma \sum_{t=1}^{3} \sum_{\alpha=1}^{l} \frac{t |\tilde{\mu}_\alpha^{(t)}|^2}{(\omega - \epsilon_{\alpha,t})^2 + \Gamma^2}, \tag{D6}$$

where the dipole transition moment for symmetric exciton is $\tilde{\mu}_\alpha^{(t)} = \Sigma_{\bar{m}} \mu_{\bar{m}} \tilde{\phi}_\alpha^{(t)}(\bar{m})$. Clearly, fully symmetric excitons with $t=1$ do not contribute to Eq. (D6). For each generation, the wavefunctions are equal, and the vector sum of the transition dipoles of such an exciton is exactly zero. It follows from Eqs. (A2) and (A3) that the energies and wavefunctions of excitons with index $t=2$ and $t=3$ are identical. We thus obtain from Eq. (D6),

$$\sigma_s(\omega) = 2\Gamma \sum_{\alpha=1}^{l} \frac{|\tilde{\mu}_\alpha^{(2)}|^2}{(\omega - \epsilon_{\alpha,2})^2 + \Gamma^2}. \tag{D7}$$

Using the wavefunction properties for the $t=2$ exciton and the relative orientation of the dipoles μ_m along the segments, we can prove by induction that

$$\tilde{\mu}_\alpha^{(2)} = \frac{3i}{2} \sum_{j=1}^{l} \tilde{\phi}_\alpha^{(2)}(j)(\mathbf{e}_x \mp i \mathbf{e}_y), \tag{D8}$$

where $\mathbf{e}_y$ is the unit vector, parallel to the symmetry axis $A_{\bar{m}}$, which goes through exciton origin (parallel to ordinate axis in the bottom panel of Fig. 5). The direction of $\mathbf{e}_x$ is chosen similarly to $\mathbf{e}_x^{(s)}$; it is perpendicular to $\mathbf{e}_y$.

When $q_t \neq 1$, system (A2) is equivalent to system (A1) for the antisymmetric excitons of length l, thus, $\tilde{\phi}_\alpha^{(2)} \equiv \phi_\alpha^{(l)}$ and $\epsilon_{\alpha,2} \equiv \epsilon_\alpha^{(l)}$, so that $\tilde{\mu}_\alpha^{(s)} = \mu_\alpha^{(l)}$. Finally, by substituting Eq. (A13) in Eq. (D8) and using definition Eq. (D5), we obtain for the ''symmetric'' part of the absorption,

$$\sigma_s(\omega) = \frac{4}{3} \Gamma \sum_{\alpha=1}^{l} \frac{|\mathbf{M}_\alpha^{(l)}|^2}{(\omega - \epsilon_\alpha^{(l)})^2 + \Gamma^2}. \tag{D9}$$

[1] R. Lecuiller, J. Berrehar, C. Lapersonne-Meyer, and M. Schott, Phys. Rev. Lett. **80**, 4068 (1998).
[2] B. Kraabel, D. Hulin, C. Aslangul, C. Lapersonne-Meyer, and M. Schott, J. Chem. Phys. **227**, 83 (1998).
[3] J. Berrehar, J. L. Fave, C. Lapersonne, M. Schott, and M. Eckhardt, Mol. Cryst. Liq. Cryst. **117**, 393 (1985).
[4] D. A. Tomalia, A. M. Naylor, and W. A. Goddard, Angew. Chem. Int. Ed. Engl. **29**, 138 (1990); M. K. Lothian-Tomalia, D. M. Hedstrand, D. A. Tomalia, A. B. Padias, and H. K. Hall, Jr., Tetrahedron **53**, 15,495 (1997).
[5] D.-L. Jiang and T. Aida, Nature (London) **388**, 454 (1997).
[6] V. Balzani, S. Campagna, G. Denti, A. Juris, S. Serroni, and M. Venturi, Acc. Chem. Res. **31**, 26 (1998); M. Venturi, S. Serroni, A. Juris, S. Campagna, and V. Balzani, Top. Curr. Chem. **197** (Springer, Berlin, 1998).
[7] J. Freéchet, Science **263**, 1710 (1994).
[8] S. Mattei, P. Wallimann, B. Kenda, W. Amrein, and F. Diederich, Helv. Chim Acta **80**, 2391 (1997); D. K. Smith and F. Diederich, Chem.-Eur. J. **4**, 1353 (1998).
[9] F. Diederich and C. Thilgen, Science **271**, 317 (1996); D. Armspach, E. C. Constable, F. Diederich, C. E. Housecroft, and J. F. Nierengarten, Chem. Commun. (Cambridge) **17**, 2009 (1996).
[10] J. F. Nierengarten, T. Habicher, P. Kessinger, F. Cardullo, F. Diederich, V. Gramlich, J. P. Gisselbrecht, C. Boudon, and M. Gross, Helv. Chim Acta **80**, 2238 (1997); C. Boudon, J. P. Gisselbrecht, M. Gross, A. Herrmann, M. Ruttimann, J. Crassous, F. Cardullo, L. Echegoyen, and F. Diederich, J. Am. Chem. Soc. **120**, 7860 (1998).
[11] R. J. Pieters and F. Diederich, Chem. Commun. (Cambridge) **19**, 2255 (1996); R. J. Pieters, J. Cuntze, M. Bonnet, and F. Diederich, J. Chem. Soc., Perkin Trans. 2 **10**, 1891 (1997).
[12] D. Armspach, E. C. Constable, F. Diederich, C. E. Housecroft, J. F. Nierengarten, Chem.-Eur. J. **4**, 723 (1998).
[13] S. R. Forrest, Chem. Rev. **97**, 1793 (1997).
[14] J. Chem. Phys. (Special Issue on Light-Harvesting Physics Workshop), **107** (1997); V. Sundström and R. van Grondelle, in *Anoxygenic Photosynthetic Bacteria*, edited by R. E. Blankenship, M. T. Madiga, and C. E. Baner (Kluwer Academic, Dordrecht, 1995), p. 349.
[15] J. Deisenhofer, O. Epp, K. Miki, R. Huber, and H. Michel, Nature (London) **318**, 618 (1985).
[16] U. Ermler, G. Fritzsch, S. K. Buchanan, and H. Michel, Structure **2**, 925 (1994).

[17] G. McDermott, S. Prince, A. Freer, A. Hawthornthwaite-Lawless, M. Papiz, R. Cogdell, and N. Isaacs, Nature (London) **318**, 618 (1985).
[18] J. Koepke, X. C. Hu, C. Münke, K. Schulten, and H. Michel, Structure **4**, 581 (1996).
[19] J. Michl and V. Bonacic-Koutecky, *Electronic Aspects of Organic Photochemistry* (Wiley, New York, 1990); M. Klessinger and J. Michl, *Excited States and Photochemistry of Organic Molecules* (VCH, New York, 1995).
[20] S. Speiser, Chem. Rev. **96**, 1953 (1996).
[21] D. R. Kanis, M. A. Ratner, and T. J. Marks, Chem. Rev. **94**, 195 (1994).
[22] J. L. Brédas, C. Adant, P. Tackyx, A. Persoons, and B. M. Pierce, Chem. Rev. **94**, 243 (1994).
[23] A. S. Davydov, *Theory of Molecular Excitons* (Plenum, New York, 1971).
[24] *Excitons*, edited by E. I. Rashba and M. D. Sturge (North-Holland, Amsterdam, 1982); V. B. Broude, E. I. Rashba, and E. F. Sheka, *Spectroscopy of Molecular Excitons* (Springer, Berlin, 1985).
[25] S. Tretiak, V. Chernyak, and S. Mukamel, J. Am. Chem. Soc. **119**, 11,408 (1997).
[26] S. Tretiak, V. Chernyak, and S. Mukamel, J. Chem. Phys. **105**, 8914 (1996).
[27] S. Mukamel, S. Tretiak, T. Wagersreiter, and V. Chernyak, Science **277**, 781 (1997).
[28] S. Tretiak, V. Chernyak, and S. Mukamel, J. Phys. Chem. B **102**, 3310 (1998).
[29] R. Kopelman, M. R. Shortreed, Z.-Y. Shi, W. Tan, Z. Xu, C. Devadoss, J. S. Moore, A. Bar-Haim, and Y. Klafter, Phys. Rev. Lett. **78**, 1239 (1997).
[30] A. Bar-Haim, Y. Klafter, and R. Kopelman, J. Am. Chem. Soc. **119**, 6197 (1997).
[31] M. R. Shortreed, S. F. Swallen, Z.-Y. Shi, W. Tan, Z. Xu, J. S. Moore, and R. Kopelman, J. Phys. Chem. B **101**, 6318 (1997).
[32] M. Shortreed, Z.-Y. Shi, and R. Kopelman, Mol. Cryst. Liq. Cryst. Sci. Technol., Sect. A **283**, 95 (1996).
[33] Y. Tanizaki, H. Inoue, T. Hoshi, and J. Shiraishi, Z. Phys. Chem., Neue Folge **74**, 45 (1971); Y. Hirata, T. Okada, N. Mataga, and T. Nomoto, J. Phys. Chem. **96**, 6559 (1992).
[34] Z. Xu, M. Kahr, K. L. Walker, C. L. Wilkins, and J. S. Moore, J. Am. Chem. Soc. **116**, 4537 (1994).
[35] S. Mukamel, *Principles of Nonlinear Optical Spectroscopy* (Oxford University Press, Oxford, 1995).
[36] J. A. Pople and G. A. Segal, J. Chem. Phys. **43**, S136 (1965).
[37] J. A. Pople, D. L. Beveridge, and P. Dobosh, J. Chem. Phys. **47**, 2026 (1967).
[38] J. Ridley and M. C. Zerner, Theor. Chim. Acta **32**, 111 (1973).
[39] M. C. Zerner, G. H. Loew, R. F. Kirchner, and U. T. Mueller-Westerhoff, J. Am. Chem. Soc. **102**, 589 (1980).
[40] R. McWeeny and B. T. Sutcliffe, *Methods of Molecular Quantum Mechanics* (Academic, New York, 1976).
[41] E. R. Davidson, *Reduced Density Matrices in Quantum Chemistry* (Academic, New York, 1976).
[42] M. R. Shortreed, Ph.D. thesis, U. of Michigan (1996), p. 131.
[43] A. A. Kirillov, *Elements of the Theory of Representations* (Springer, Berlin, 1986).
[44] E. N. Economou, *Green's Functions in Quantum Physics* (Springer, New York, 1994).
[45] D. Thouless, Phys. Rep., Phys. Lett. **13C**, 93 (1974).
[46] F. C. Spano, J. R. Kuklinski, and S. Mukamel, Phys. Rev. Lett. **65**, 211 (1990).
[47] *J-aggregates*, edited by T. Kobayaschi (World Scientific, Singapore, 1996).
[48] X. Hu, T. Ritz, A. Damjanović, and K. Schulten, J. Phys. Chem. B **101**, 3854 (1997); X. Hu, A. Damjanović, T. Ritz, and K. Schulten, Proc. Natl. Acad. Sci. USA **95**, 5935 (1998).
[49] X. Hu and K. Schulten, Phys. Today **50**, 28 (1997).
[50] T. Meier, Y. Zhao, V. Chernyak, and S. Mukamel, J. Chem. Phys. **107**, 3876 (1997).
[51] J. Feder, *Fractals* (Plenum, New York, 1988).
[52] As discussed in Sec. III A, the wavefunctions of different branches scale to each other as $(1,q_t,q_t^2)$ for a given $\tilde{\phi}_\alpha^{(t)}$.
[53] A. O. Barut and R. Raczka, *Theory of Group Representations and Applications* (World Scientific, Singapore, 1986).